SUPPORTING INFORMATION

A journey towards the forbidden zone: a new, cold, *UHP* unit in the Dora-Maira Massif (Western Alps)

Paola Manzotti[1*], Federica Schiavi[2], Francesco Nosenzo[1], Pavel Pitra[3,4], Michel Ballèvre[3]

Affiliations:

[1] Department of Geological Sciences, Stockholm University, 106 91 Stockholm, Sweden

[2] Université Clermont Auvergne, CNRS, IRD, OPGC, Laboratoire Magmas et Volcans, 63000 Clermont-Ferrand, France

[3] Univ Rennes, CNRS, Géosciences Rennes – UMR 6118, F–35000 Rennes, France

[4] Česká geologická služba (Czech geol. survey), CZ-118 21 Prague 1, Czech Republic

*Correspondence: paola.manzotti@geo.su.se Tel. +46 (0)8 16 4745, ORCID: 0000-0002-6945-9878

Laboratory
University of Lausanne

Instrument
JEOL JXA-8530F equipped with five WDS spectrometers

Operating conditions for spot analyses
15 kV accelerating voltage, 15 nA beam current, spot size: focused for gr, 5 μm for ctd φ(ρZ) matrix correction was applied based on Armstrong (1988) and Armstrong (1991)

Analysed mineral		
garnet, chloritoid		
Standard	**Counting time (peak)**	**Counting time (background)**
wollastonite: Si, Ca	30	15
orthoclase: K	20	10
andalusite: Al	30	15
olivine (forsterite): Mg	30	15
tephroite: Mn	30	15
olivine (fayalite): Fe	30	15
albite: Na	20	10
ilmenite: Ti	30	15

Operating conditions for garnet X-ray maps
15 kV accelerating voltage, 100 nA beam current, 40 ms on 1 micron pixel

Laboratory
University of Lausanne

Instrument
JEOL JXA-8530F equipped with five WDS spectrometers

Operating conditions for spot analyses
15 kV accelerating voltage, 15 nA beam current, spot size = 5 μm. φ(ρZ) matrix correction was applied based on Armstrong (1988) and Armstrong (1991)

Analysed mineral		
muscovite, paragonite, chlorite		
Standard	**Counting time (peak)**	**Counting time (background)**
orthoclase: Si	30	15
orthoclase: K	20	10
anorthite: Al	30	15
anorthite: Ca	30	15
olivine (forsterite): Mg	30	15
tephroite: Mn	30	15
olivine (fayalite): Fe	30	15
albite: Na	20	10
ilmenite: Ti	30	15
phlogopite: F	30	15

Laboratory
University of Lausanne

Instrument
JEOL JXA-8530F equipped with five WDS spectrometers

Operating conditions for spot analyses
15 kV accelerating voltage, 15 nA beam current, spot size = 3 μm. φ(ρZ) matrix correction was applied based on Armstrong (1988) and Armstrong (1991)

Analysed mineral		
epidote		
Standard	**Counting time (peak)**	**Counting time (background)**
wollastonite: Si	30	15
orthoclase: K	20	10
andalusite: Al	30	15
wollastonite: Ca	30	15
olivine (forsterite): Mg	30	15
tephroite: Mn	30	15
olivine (fayalite): Fe	30	15
albite: Na	20	10
ilmenite: Ti	30	15

Laboratory
University of Lausanne

Instrument
JEOL JXA-8530F equipped with five WDS spectrometers

Operating conditions for spot analyses
15 kV accelerating voltage, 10 nA beam current, spot size = 5 μm φ(ρZ) matrix correction was applied based on Armstrong (1988) and Armstrong (1991)

Analysed mineral		
carbonate		
Standard	**Counting time (peak)**	**Counting time (background)**
olivine (forsterite): Mg	10	5
strontianite: Sr	30	15
tephroite: Mn	30	15
calcite: Ca	30	15
olivine (fayalite): Fe	30	15

Laboratory
Microsonde Ouest, Brest (France)

Instrument
Cameca SX100 equipped with 5 WDS spectrometers

Operating conditions for spot analyses
15 kV accelerating voltage, 20 nA beam current, spot size = 1 μm. φ(ρZ) matrix correction was applied based on Pouchou and Pichoir (1985)

Analysed mineral		
garnet		
Standard	**Counting time (peak)**	**Counting time (background)**
albite: Na, Si	10	5
orthoclase: K	10	5
corundum: Al	10	5
wollastonite: Ca	10	5
forsterite: Mg	10	5
$MnTiO_3$: Mn, Ti	30	15
andradite: Fe	10	5
Cr_2O_3: Cr	10	5
NiO: Ni	10	5

Operating conditions for X-ray maps
15 kV accelerating voltage, 20 nA beam current, 0,1 s on 6μm pixel for garnet of Fig.7
15 kV accelerating voltage, 20 nA beam current, 0,1 s on 5μm pixel for garnet of Fig.8

Tab. S1 Operating conditions for microprobe analyses

Mineral abbreviations	
ab	albite
alm	almandine
am	amphibole
bi	biotite
car	carpholite
chl	chlorite
coe	coesite
ctd	chloritoid
ep	epidote
g	garnet
gl	sodic amphibole
gph	graphite
grs	grossular
hb	hornblende
ilm	ilmenite
jd	jadeite
ky	kyanite
law	lawsonite
mu	muscovite
pa	paragonite
pl	plagioclase
prp	pyrope
q	quartz
ru	rutile
spss	spessartine
sph	titanite
ta	talc
tur	tourmaline

Other symbols (mole/atomic proportions)		
X_{Mn}	Mn/(Mn + Fe + Mg)	for chl, ctd
X_{Mg}	Mg/(Fe + Mg)	for g, chl, ctd, mu
alm	$Fe^{2+}/(Fe^{2+} + Mg + Ca + Mn)$	
spss	$Mn/(Fe^{2+} + Mg + Ca + Mn)$	
prp	$Mg/(Fe^{2+} + Mg + Ca + Mn)$	
grs	$Ca/(Fe^{2+} + Mg + Ca + Mn)$	
X_{Na}	Na/(Na + K)	for mu
a.p.f.u.	atom per formula unit	
wt%	weight per cent	
mol.%	mole per cent	
vol. %	volume per cent	

Tab. S2 Mineral abbreviations and other symbols used in this study

Mineral	g	g	g	g	g	g	g	g	g	g	g	g	g	g	g	g	ep	ep
Zone	rim	rim	rim	outer core	outer core	inner core	inner core	inner core	outer core	outer core	outer core	rim	rim	outer core, close to coe (Fig. 7)	outer core, close to coe (Fig. 8)	outer core, close to coe (Fig. 6)	rim, close to q	replacing law in g core	replacing law in g rim
Analysis	4	9	23	36	43	73	77	79	133	162	174	189	193	1	11	13	5	3	8
SiO_2	36.86	37.25	37.18	36.83	36.92	36.69	36.51	36.50	36.82	36.77	36.79	37.24	37.48	37.20	37.27	37.01	37.41	38.43	38.35
TiO_2	0.09	0.06	0.08	<0.01	0.07	0.07	0.06	0.07	0.06	0.04	0.06	0.12	0.11	0.02	0.03	0.02	0.14	0.08	0.09
Cr_2O_3	<0.01	<0.01	<0.01	<0.01	<0.01	<0.01	<0.01	<0.01	<0.01	0.01	<0.01	0.01	<0.01	<0.01	<0.01	<0.01	<0.01	<0.01	<0.01
NiO	0.02	<0.01	<0.01	<0.01	<0.01	0.05	0.03	0.03	<0.01	0.01	<0.01	<0.01	<0.01	<0.01	<0.01	<0.01	<0.01	<0.01	<0.01
Al_2O_3	21.06	21.19	21.00	21.15	21.19	20.96	20.89	20.95	21.24	20.94	21.17	21.33	21.03	20.90	20.59	20.88	20.59	31.32	29.26
FeO	32.44	29.26	32.43	36.26	35.25	33.91	34.23	33.88	35.79	36.48	36.03	31.15	30.40	36.59	36.77	36.27	32.36	3.51	5.74
MnO	0.48	0.52	0.90	3.09	3.48	5.29	5.06	5.17	3.14	2.17	1.58	0.59	0.51	2.60	2.55	2.64	0.90	0.10	0.27
MgO	0.78	0.72	1.32	1.82	1.74	1.41	1.46	1.47	1.69	1.97	2.12	0.94	0.83	1.87	1.85	1.84	1.42	0.03	0.03
CaO	8.57	10.84	7.42	2.01	2.09	1.96	1.89	1.89	1.95	2.24	2.66	9.23	10.05	2.19	2.10	2.08	7.60	23.60	24.06
Na_2O	<0.01	0.03	0.03	0.01	0.08	0.12	0.09	0.09	0.02	<0.01	0.01	0.03	0.09	0.04	0.02	0.04	0.02	<0.01	<0.01
K_2O	<0.01	0.01	0.00	<0.01	<0.01	<0.01	<0.01	0.01	<0.01	<0.01	0.01	<0.01	<0.01	<0.01	<0.01	0.01	<0.01	<0.01	<0.01
Total	100.30	99.88	100.36	101.17	100.82	100.47	100.22	100.06	100.71	100.63	100.44	100.64	100.50	101.41	101.18	100.79	100.44	97.07	97.80
Oxygen-equivalents	12	12	12	12	12	12	12	12	12	12	12	12	12	12	12	12	12	12.5	12.5
Si	2.96	2.98	2.98	2.96	2.97	2.97	2.97	2.97	2.97	2.97	2.96	2.97	2.99	2.98	3.00	2.98	3.00	2.96	2.96
Ti	0.01	0.01	0.00	0.00	0.00	0.00	0.00	0.00	0.00	0.00	0.00	0.01	0.01	0.00	0.00	0.00	0.01	0.00	0.00
Cr	0.00	0.00	0.00	0.00	0.00	0.00	0.00	0.00	0.00	0.00	0.00	0.00	0.00	0.00	0.00	0.00	0.00	0.00	0.00
Ni	0.00	0.00	0.00	0.00	0.00	0.00	0.00	0.00	0.00	0.00	0.00	0.00	0.00	0.00	0.00	0.00	0.00	0.00	0.00
Al	1.99	2.00	1.98	2.00	2.01	2.00	2.00	2.01	2.02	1.99	2.01	2.00	1.98	1.97	1.95	1.98	1.94	2.85	2.66
Fe^{3+}	0.08	0.03	0.05	0.08	0.05	0.06	0.08	0.06	0.03	0.07	0.06	0.05	0.05	0.07	0.06	0.06	0.05	0.23	0.37
Fe^{2+}	2.10	1.92	2.12	2.36	2.33	2.23	2.25	2.24	2.38	2.39	2.37	2.03	1.98	2.38	2.42	2.39	2.11	0.00	0.00
Mn	0.03	0.04	0.06	0.21	0.24	0.36	0.35	0.36	0.21	0.15	0.11	0.04	0.03	0.18	0.17	0.18	0.06	0.01	0.02
Mg	0.09	0.09	0.16	0.22	0.21	0.17	0.18	0.18	0.20	0.24	0.25	0.11	0.10	0.22	0.22	0.22	0.17	0.00	0.00
Ca	0.74	0.93	0.64	0.17	0.18	0.17	0.16	0.16	0.17	0.19	0.23	0.79	0.86	0.19	0.18	0.18	0.65	1.95	1.99
Na	0.00	0.01	0.01	0.00	0.01	0.02	0.01	0.01	0.00	0.00	0.00	0.00	0.00	0.01	0.00	0.01	0.00	0.00	0.00
K	0.00	0.00	0.00	0.00	0.00	0.00	0.00	0.00	0.00	0.00	0.00	0.00	0.00	0.000	0.00	0.00	0.00	0.00	0.00
Total	8.00	8.00	8.00	8.00	8.00	7.98	8.00	7.99	7.98	8.00	8.00	8.00	8.00	8.00	8.00	8.00	7.99	8.00	8.00
X_{Mg}	0.04	0.04	0.07	0.09	0.08	0.07	0.07	0.07	0.08	0.09	0.10	0.05	0.05	0.08	0.08	0.08	0.07		
alm	71	64	71	80	79	76	77	76	80	80	80	68	67	80	81	80	71		
prp	3	3	5	7	7	6	6	6	7	8	9	4	3	7	7	7	6		
grs	25	31	21	6	6	6	5	5	6	6	8	27	29	6	6	6	22		
spss	1	1	2	7	8	12	12	12	7	5	4	1	1	6	6	6	2		

Tab. S3 Representative mineral analyses and formulas of garnet and epidote in the garnet-chloritoid micaschist CH11. Garnet analyses (from analysis n. 4 to analysis n. 193) are selected along the A-B profile indicated in Figure 7a

Mineral	**ctd**	**ctd**	**ctd**	**ctd**	**ctd**	**ctd**	**ctd**	**ctd**	**chl**	**chl**
Zone	inclusion in g inner core	inclusion in g inner core	inclusion in g outer core	inclusion in g outer core	core	core	rim	rim	replacing g	overgrowing the main S
Analysis	21	38	7	11	22	17	28	20	10	32
SiO_2	24.22	24.19	24.41	24.27	24.52	24.32	24.24	24.21	24.62	24.70
TiO_2	0.01	0.01	0.02	<0.01	0.01	0.48	0.01	<0.01	0.07	0.05
Al_2O_3	40.04	40.33	40.40	40.17	40.43	40.26	39.83	39.66	20.98	21.03
FeO	24.49	24.82	23.88	24.14	23.90	24.52	25.62	26.23	33.52	32.72
MnO	0.45	0.39	0.14	0.12	0.12	0.15	0.06	0.14	0.09	0.09
MgO	2.33	2.29	2.86	2.83	2.93	2.81	1.94	1.56	8.60	9.20
CaO	0.01	<0.01	<0.01	<0.01	0.01	<0.01	0.01	<0.01	0.01	0.01
Na_2O	<0.01	<0.01	<0.01	0.01	0.01	0.01	0.02	<0.01	<0.01	0.01
K_2O	0.01	<0.01	<0.01	0.01	<0.01	<0.01	0.02	<0.01	<0.01	0.01
Total	91.56	92.03	91.71	91.55	91.93	92.55	91.75	91.80	87.89	87.82
Oxygen-equivalents	14	14	14	14	14	14	14	14	14	14
Si	2.02	2.01	2.03	2.02	2.03	2.01	2.03	2.03	2.71	2.70
Ti	0.00	0.00	0.00	0.00	0.00	0.03	0.00	0.00	0.01	0.00
Al	3.94	3.96	3.95	3.94	3.94	3.92	3.93	3.93	2.72	2.71
Fe^{2+}	1.71	1.73	1.66	1.68	1.65	1.69	1.79	1.84	3.08	3.00
Mn	0.03	0.03	0.01	0.01	0.01	0.01	0.00	0.01	0.01	0.01
Mg	0.29	0.28	0.35	0.35	0.36	0.35	0.24	0.19	1.41	1.50
Ca	0.00	0.00	0.00	0.00	0.00	0.00	0.00	0.00	0.00	0.00
Na	0.00	0.00	0.00	0.00	0.00	0.00	0.00	0.00	0.00	0.00
K	0.00	0.00	0.00	0.00	0.00	0.00	0.00	0.00	0.00	0.00
Total	7.99	8.01	8.00	8.00	7.99	8.01	7.99	8.00	9.94	9.92
X_{Mg}	0.15	0.14	0.17	0.17	0.18	0.17	0.12	0.09	0.31	0.33
X_{Mn}	0.015	0.015	0.005	0.005	0.005	0.005	0.000	0.005	0.002	0.002

Tab. S4 Representative mineral analyses and formulas of chloritoid and chlorite in the garnet-chloritoid micaschist CH11

Mineral	mu	mu	mu	mu	mu	mu	mu	pa	pa	pa	pa	pa	pa	pa	pa
Zone	core, matrix	core, matrix	rim, matrix	rim, matrix	prograde, inclusion in g outer core	inclusion in g, replacing law	inclusion in g, replacing law	matrix	matrix	overgrowing the main S	overgrowing the main S	prograde, inclusion in g outer core	prograde, inclusion in g outer core	inclusion in g core replacing law	inclusion in g rim replacing law
Analysis	9	28	36	26	39	53	2	2	15	16	17	37	38	7	29
SiO_2	51.40	51.77	49.98	49.67	51.93	50.04	49.25	47.15	46.96	47.14	47.21	47.49	47.62	46.89	47.17
TiO_2	0.14	0.13	0.28	0.27	0.12	0.22	0.29	0.04	0.05	0.04	0.04	0.04	0.03	0.07	0.06
Al_2O_3	27.45	26.46	28.71	29.08	27.07	28.70	29.75	40.04	40.19	40.26	39.98	39.70	40.15	39.66	40.01
FeO	2.25	2.71	3.49	3.50	2.77	3.40	4.00	0.46	0.45	0.32	0.33	0.58	0.63	0.46	0.50
MnO	<0.01	0.01	0.01	<0.01	0.01	0.01	0.02	0.01	<0.01	<0.01	<0.01	0.02	0.02	<0.01	<0.01
MgO	3.08	3.13	2.30	2.14	3.14	2.32	1.99	0.16	0.14	0.15	0.14	0.39	0.29	0.21	0.24
CaO	<0.01	<0.01	<0.01	<0.01	<0.01	0.04	0.08	0.09	0.08	0.10	0.09	0.07	0.08	0.10	0.17
Na_2O	0.18	0.09	0.36	0.34	0.15	0.44	0.42	7.42	7.16	7.14	7.17	7.30	7.31	6.97	7.19
K_2O	11.51	11.58	11.17	11.15	11.52	11.00	10.36	0.37	0.65	0.65	0.76	0.55	0.53	0.91	0.18
F	0.13	0.14	0.08	0.14	0.11	0.12	0.08	0.05	0.04	0.02	0.01	0.05	0.02	0.04	<0.01
Total	96.14	96.02	96.38	96.29	96.82	96.29	96.16	95.79	95.72	95.82	95.73	96.14	96.66	95.31	95.52
Oxygen-equivalents	11	11	11	11	11	11	11	11	11	11	11	11	11	11	11
Si	3.42	3.45	3.33	3.32	3.43	3.34	3.28	2.99	2.98	2.99	3.00	3.01	3.00	3.00	2.99
Ti	0.01	0.01	0.01	0.01	0.01	0.01	0.01	0.00	0.00	0.00	0.00	0.00	0.00	0.00	0.00
Al	2.15	2.08	2.26	2.29	2.11	2.26	2.34	3.00	3.01	3.01	2.99	2.96	2.98	2.99	2.99
Fe^{2+}	0.13	0.15	0.19	0.20	0.15	0.19	0.22	0.02	0.02	0.02	0.02	0.03	0.03	0.02	0.03
Mn	0.00	0.00	0.00	0.00	0.00	0.00	0.00	0.00	0.00	0.00	0.00	0.00	0.00	0.00	0.00
Mg	0.31	0.31	0.23	0.21	0.31	0.23	0.20	0.02	0.01	0.01	0.01	0.04	0.03	0.02	0.03
Ca	0.00	0.00	0.00	0.00	0.00	0.00	0.01	0.01	0.01	0.01	0.01	0.00	0.01	0.01	0.01
Na	0.02	0.01	0.05	0.05	0.02	0.06	0.05	0.91	0.88	0.88	0.88	0.90	0.89	0.86	0.88
K	0.98	0.990	0.95	0.95	0.97	0.94	0.88	0.03	0.05	0.05	0.06	0.04	0.04	0.07	0.01
F	0.18	0.210	0.12	0.20	0.15	0.18	0.12	0.07	0.05	0.03	0.02	0.06	0.03	0.05	0.00
Total	7.02	7.00	7.02	7.03	7.00	7.03	6.99	6.98	6.96	6.97	6.97	6.98	6.98	6.97	6.94
X_{Mg}	0.70	0.67	0.55	0.51	0.67	0.55	0.48	0.50	0.33	0.33	0.33	0.57	0.50	0.50	0.50
X_{Na}	0.02	0.01	0.05	0.05	0.02	0.06	0.05	0.97	0.95	0.95	0.94	0.96	0.96	0.92	0.99

Tab. S5 Representative mineral analyses and formulas of muscovite and paragonite in the garnet-chloritoid micaschist CH11

Sample CH11 - g-ctd micaschist	
Major elements (oxide wt.%)	
SiO_2	61.47
Al_2O_3	19.64
Fe_2O_3	6.93
MnO	0.10
MgO	1.81
CaO	0.39
Na_2O	1.12
K_2O	4.61
TiO_2	0.82
P_2O_5	< B.D.
LOI	2.86
Total	99.73

Tab. S6 Whole-rock composition for sample CH11

Software		
Theriak-Domino (de Capitani and Brown 1987; de Capitani and Petrakakis 2010)		
Thermodynamic dataset		
Holland and Powell 2011 version ds6.2		
Solution models (minerals)		
	Mineral	**Solution model**
Orthosilicates	Garnet	White et al. 2014a, 2014b
	Kyanite	pure
	Chloritoid	White et al. 2014a, 2014b
	Staurolite	White et al. 2002; Holland and Powell 2003
Disilicates	Epidote	Holland and Powell 2011
	Lawsonite	pure
Chain silicates	Clinopyroxene	Green et al. 2016
	Amphibole	Green et al. 2016
	Carpholite	Wei and Powell 2004, ideal
Sheet silicates	White mica	White et al. 2014a, 2014b
	Biotite	White et al. 2014a, 2014b
	Chlorite	White et al. 2014a, 2014b
	Talc	Holland and Powell 2011, ideal
Framework silicates	Plagioclase	Holland and Powell 2003
	Quartz/Coesite	pure
Oxydes	Rutile	pure
	Ilmenite	White et al. 2000
	Magnetite	White et al. 2002
Solution models (fluid)		
	H_2O	pure

Tab. S7 Phases and activity composition models considered in the thermodynamic calculations

Sample	CH11
Lithology	g-ctd micaschist
Thin section	CH11, CH11-1, CH11-2, CH11-3, CH11-4, CH11-5, CH11-6

Tab. S8 Details on the studied sample. Coesite was found in thin section CH11 and CH11-6. RSCM data were obtained on thin section CH11 and CH11-5 (see table S9)

Raman spectroscopy of inclusions in garnet

Mineral inclusions in garnet were identified at the Laboratoire Magmas et Volcans (Clermont-Ferrand, France) using a Renishaw inVia confocal Raman micro-spectrometer equipped with a 532.1 ± 0.3 nm diode laser, a Rayleigh rejection edge filter, a CCD detector of 1040 x 256 pixels, and a Leica DM 2500M optical microscope with a motorized XYZ stage. The analyses were carried out in back-scattered geometry using a grating of 2400 grooves/mm, a 20 μm slit aperture (high confocality setting), a ×100 microscope objective, and ~5 mW laser power on the sample. These analytical conditions result in spatial lateral resolution of ~1 μm and vertical resolution of ~2-3 μm, and a spectral resolution of 0.4 cm^{-1}. Each analysis lasted 20 seconds (i.e., 4 accumulations of 5 s). Two-dimensional Raman mapping was performed with a spacing of 2 μm and exposure time of 10 s/point (Fig. 6a). Daily calibration of the spectrometer was performed by measuring the position of Neon lines and the main peak of silicon standard (520.5 cm^{-1}). A euhedral crystal of α-quartz manufactured by the company SICN (now Gemma Quartz & Crystal, Annecy, France) was used as standard and analyzed several times (Table S11) to check analytical reproducibility during the analytical session. The room temperature was maintained at 21 ± 1 °C. The spectra were acquired in the wavenumber range ~90-1350 cm^{-1} and also in the O-H spectral region ~3000-3800 cm^{-1} if a hydrous mineral was identified. After the analysis, fitting of the peaks of quartz (Table S12), coesite and host garnet was performed using WiRE^{TM} 4.4 software.

Raman spectroscopy on carbonaceous material (RSCM) method

Regional metamorphic processes produce a gradual transformation of the organic matter present in rocks to CM (carbonaceous material). The peak *T* reached by samples can be estimated using this graphitization process; regional metamorphic *T* thus controls the degree of graphitization (Beyssac et al. 2002, 2003). Because graphitization is considered as an irreversible process, the *T* estimates are not affected by metamorphic reactions associated with retrogression. Carbonaceous material was analysed in two thin sections of the studied sample CH11. Raman spectra of CM were obtained at the Laboratoire Magmas et Volcans (Clermont-Ferrand, France) using a Renishaw inVia confocal micro-spectrometer, equipped with a 532 nm diode laser. Because RSCM can be affected by several analytical mismatches, we followed closely the analytical procedures described by Beyssac et al. (2002, 2003). Measurements were carried out on polished thin sections using a grating of 2400 grooves/mm, a 20 μm slit aperture (high confocality setting), a ×100 microscope objective, and 1-5 mW laser power on the sample surface. The laser was generally focused at 5-15 μm depth to analyse graphite that was located below different minerals and not exposed at the surface. Each

analysis consisted of 6 or 10 accumulations of 20 seconds each in the ~900-2000 cm^{-1} wavenumber range, containing the two principal vibrations of graphite. A spectrum of the mineral phase on top of graphite (mainly calcite, quartz, albite, muscovite, and chlorite) was systematically acquired in the ~90-1350 cm^{-1} wavenumber range with an acquisition time of 15 s. On each sample, we measured at least 15-20 different grains of graphite. The spectra were processed using the WiRE^{TM} 4.4 software: first, they were truncated, then a linear baseline correction was applied in the 1200-1800 cm^{-1} spectral range, and finally curve fitting was performed. Three bands (corresponding to G, D1, and D2 components, respectively at ~1580, ~1350, and ~1620 cm^{-1}) were necessary to fit the graphite spectrum. The degree of organization of CM is quantified by the relative area of the G, D1, and D2 components of CM in Raman spectra. This is equal to D1/(G + D1 + D2) and it is defined as the peak area ratio (R2 ratio; Beyssac et al. 2002, 2003).

	Thin section	n	R2	T (°C)	SD	Confidence
sample CH11 **g-ctd micaschist**	CH11 (coe)	21	0.15–0.44	486	19	8
	CH11-5 (q)	21	0.31–0.45	481	15	6
	Average	42	0.15–0.45	483	17	5

Tab. S9 RSCM results (number of Raman spectra, R2 ratio, RSCM temperature, standard deviation, and confidence) from the g-ctd micaschist sample CH11

Garnet fractionation

Very high-resolution plane-polarised photomicrographs of the entire thin sections have been acquired with a Nikon Super Coolscan 9000 ED (Stockholm University). The modal amount of garnet was estimated in each thin section, measuring the garnet surface with respect to the surface of the entire thin section. In the seven studied thin sections, garnet modal amount ranges between 0.5 and 11%, with an average of 5% (Table S10). The modal amount of garnet inner and outer cores has been estimated on the basis of backscattered images and X-ray maps using a graphic software (Adobe Photoshop). X-ray maps were acquired on selected garnet porphyroblasts. On the basis of this analysis, 3 vol.% of garnet inner cores and 1 vol.% of garnet outer cores have been fractionated

for modelling the garnet growth in the studied sample. Representative chemical compositions of garnet inner and outer cores were subtracted from the measured bulk composition in proportion to the modal amount of the garnet inner and outer cores. The modal amount of garnet rims has been estimated on the basis of their easily identifiable pinkish colour. In addition, the relative proportion of garnet rims with respect to garnet inner and outer cores has been also estimated on backscattered images of garnet porphyroblasts from the seven thin sections, using a graphic software (Adobe Photoshop). Because there is no evidence that the andradite component is concentrated in the garnet core with respect to the garnet rim the ratio FeO/Fe_2O_3 in the bulk is considered constant.

Thin section	g modal amount (vol.%)
CH11	11
CH11-1	0.5
CH11-2	8
CH11-3	2
CH11-4	7
CH11-5	4
CH11-6	3
Average g modal amount: 5 vol.%	
Average g cores modal amount: 3 vol.%	
Average g mantles modal amount: 1 vol.%	

Tab. S10 Modal amount of garnet in the studied sample

Fig. S1 Photograph of the Chasteiran village. The studied outcrop is located immediately to the left of the Chasteiran church. We hope that the geological community will take care of this outcrop (in the middle of a nice mountain village) and preserve it from excessive hammering

Fig. S2 Photograph of the studied sample (CH11)

Fig. S3 Photomicrograph (plane-polarised light) of the thin section CH11

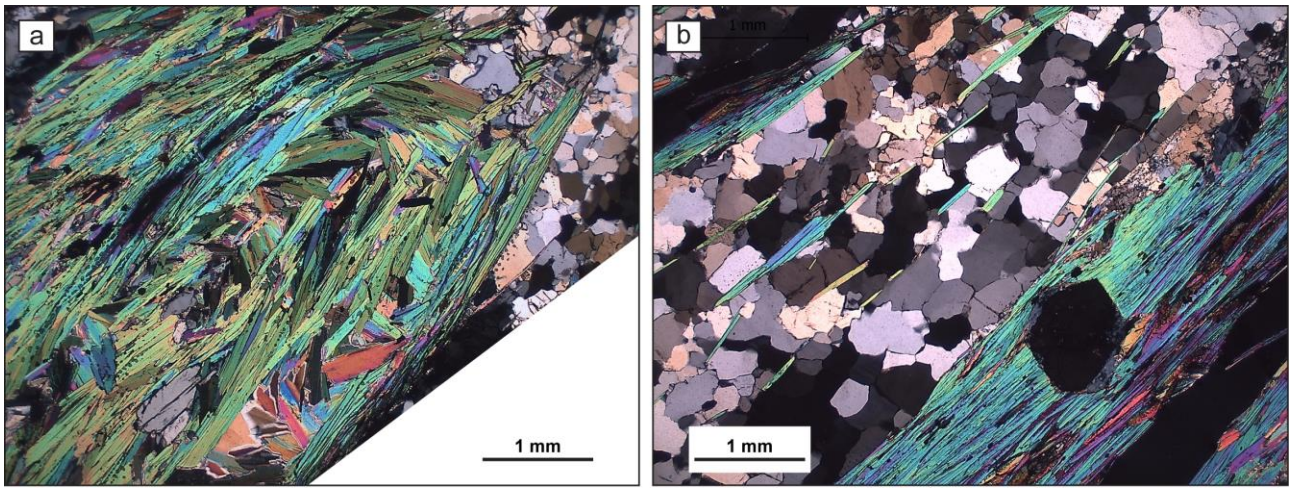

Fig. S4 Photomicrographs (cross-polarised light) for sample CH11 **a** An earlier fabric (S_1) is defined by the shape preferred orientation of muscovite and is folded (thin section CH11-1). **b** The main foliation S_2 is marked by quartz lenses and muscovite layers (thin section CH11-2)

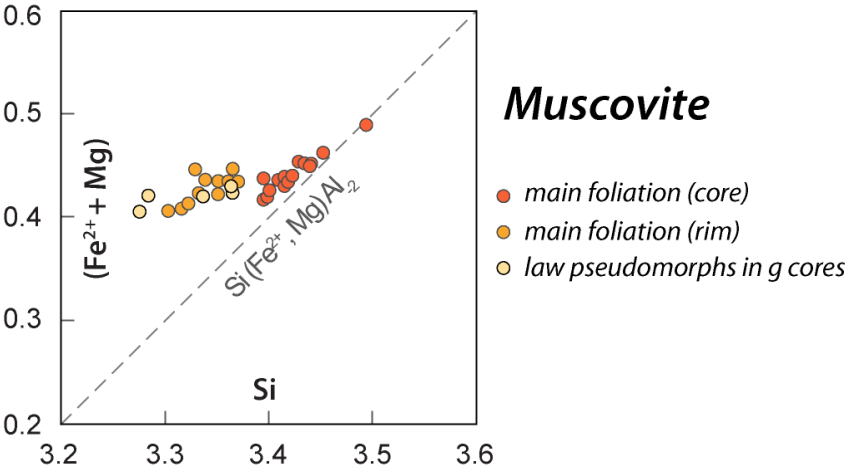

Fig. S5 Potassic white mica composition plotted in the Si vs Fe^{2+} + Mg (a.p.f.u.) diagram from the studied sample. The dashed line represents the ideal celadonitic substitution

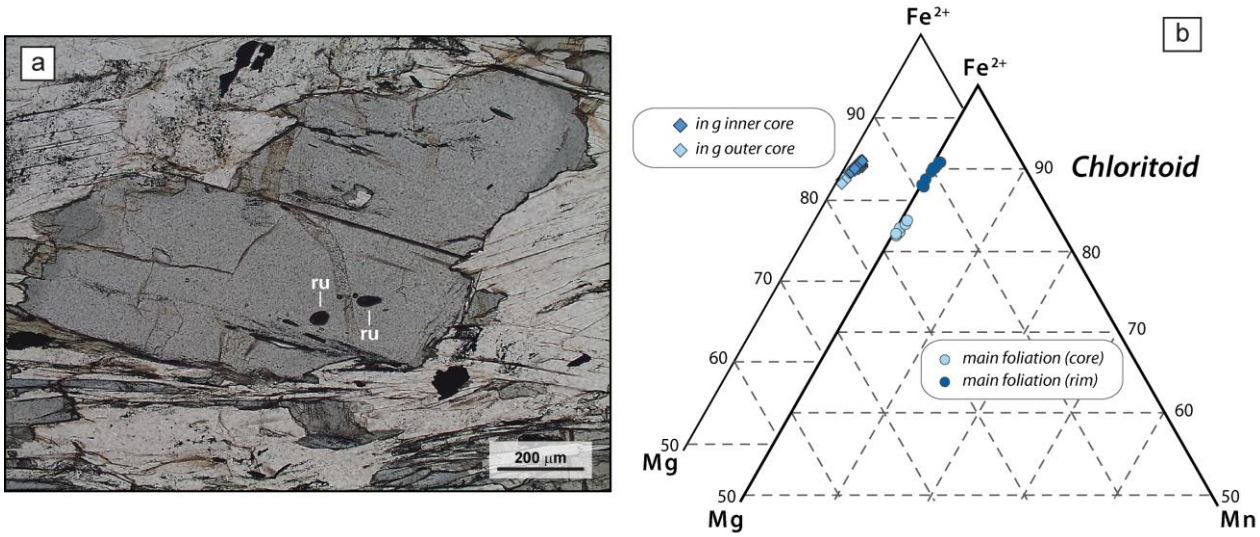

Fig. S6 a Photomicrograph (plane-polarised light) of pale blue chloritoid crystals displaying thin dark blue rims due to their higher Fe^{2+} content (thin section CH11-3). A few rutile inclusions occur in the core of the crystals. **b** Fe–Mn–Mg ternary diagrams showing the compositions of chloritoid in the studied sample

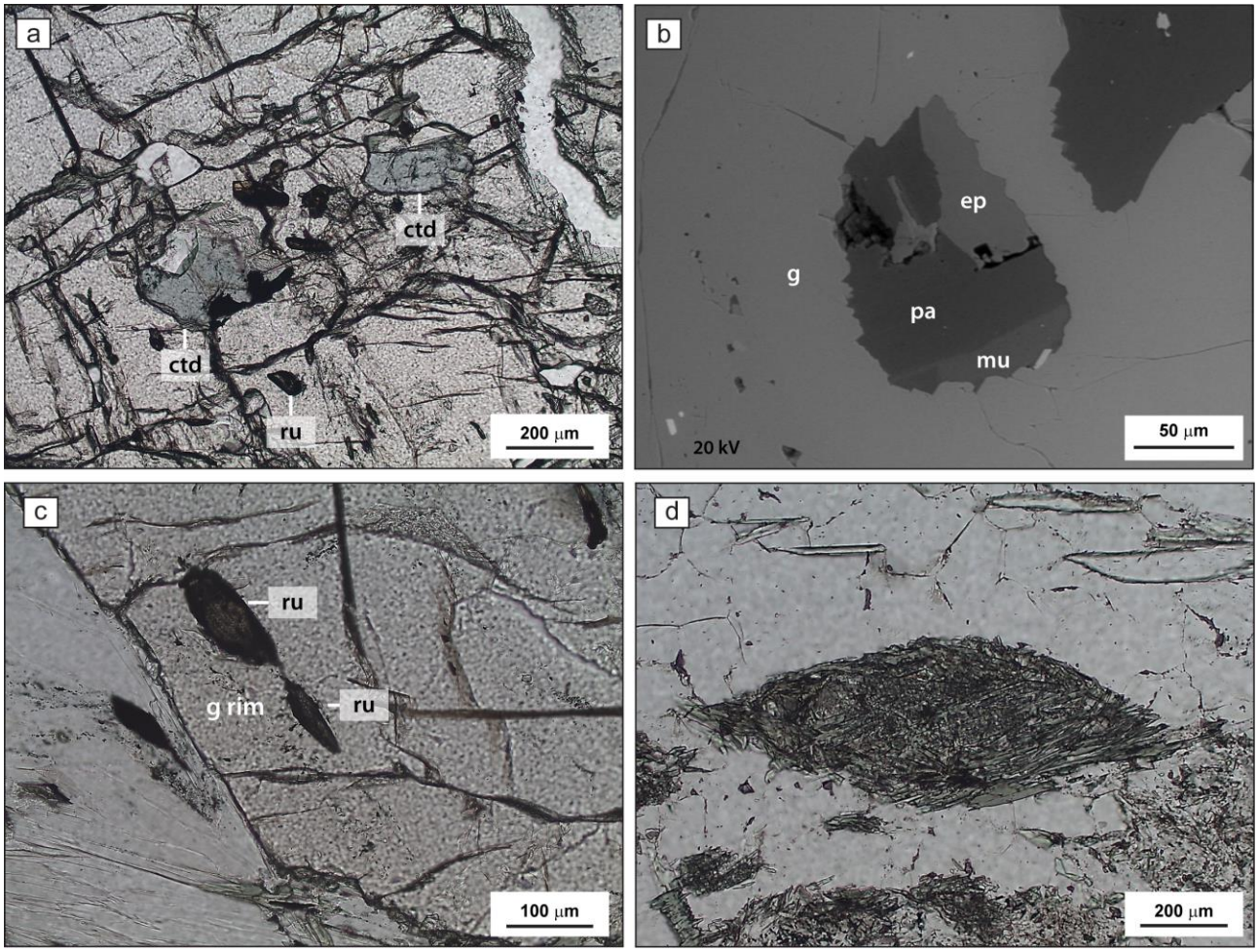

Fig. S7 a Details on the garnet inner core shown in Figures 4 and 7 (thin section CH11). Inclusions of chloritoid, rutile, and quartz in the garnet inner core (plane-polarised light). **b** An aggregate of paragonite + epidote + muscovite is included in garnet inner core and is interpreted to be a pseudomorph after lawsonite (thin section CH11-3). **c** Inclusions of rutile occur in the garnet rim (plane-polarised light, thin section CH11-3). **d** An aggregate of chlorite + albite + quartz with a characteristic rhomboidal shape, most probably derived from glaucophane crystal (plane-polarised light, thin section CH11)

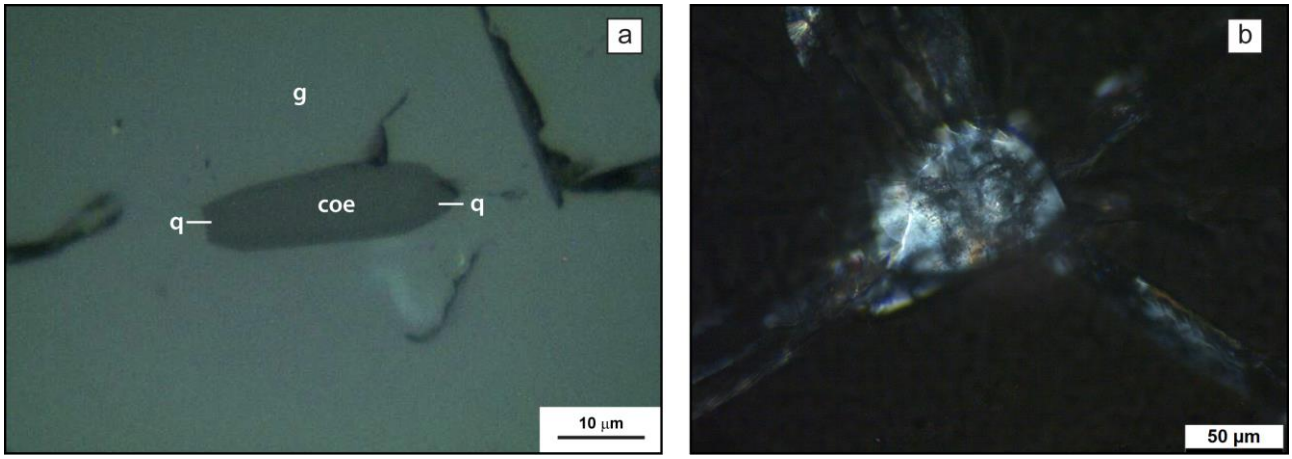

Fig. S8: a Reflected light photomicrograph of a coesite inclusion with a thin (darker) rim of quartz. **b** A coesite inclusion partially transformed to quartz (cross-polarised light). On the top right part of the inclusion, quartz replacing coesite displays palisade texture.

Standard.spot	128 measured	206 measured	464 measured	ω1	ω2
	(cm^{-1})	(cm^{-1})	(cm^{-1})	(cm^{-1})	(cm^{-1})
std.1	128.18	206.97	464.25	257.28	78.79
std.2	128.11	206.92	464.19	257.27	78.81
std.3	128.01	206.85	464.19	257.34	78.84
Average	**128.10**	**206.91**	**464.21**	**257.30**	**78.81**
STDEV	**0.08**	**0.06**	**0.04**	**0.04**	**0.03**

Tab. S11 Data of Raman shift of α-quartz. $\varpi_1 = \nu_{464} - \nu_{206}$; $\varpi_2 = \nu_{206} - \nu_{218}$

Tab. S12 Raman spectroscopy of quartz grains included in garnet. The Raman shift wavenumbers are the differences between the wavenumbers of the exciting radiation (i.e., the Rayleigh peak at 0 cm^{-1}) and Raman radiation. The analyses acquired around coesite inclusion and the analysis displaying the largest measured relative Raman shift are reported in bold. $\Delta\nu_1 = 206_{measured} - 206_{std}$; $\Delta\nu_2 = 464_{measured}\text{-}464_{std}$; $\Delta\varpi_1 = (464_{std}\text{-}205_{std}) - (464_{measured}\text{-}206_{measured})$; $\Delta\varpi_2 = (206_{std}\text{-}128_{std}) - (206_{measured}\text{-}128_{measured})$

Thin section	Domain	128 $_{measured}$ (cm^{-1})	206 $_{measured}$ (cm^{-1})	464 $_{measured}$ (cm^{-1})	ω1 (cm^{-1})	ω2 (cm^{-1})	Δω1 (cm^{-1})	Δω2 (cm^{-1})	$\Delta\nu_1$ (cm^{-1})	$\Delta\nu_2$ (cm^{-1})	Inclusion.spot
CH11	g inner core	128.62	207.28	464.73	257.45	78.66	-0.15	-0.15	0.37	0.52	g1_site3_incl1_pt1
CH11	g inner core	128.60	207.41	464.73	257.33	78.81	-0.03	0.00	0.49	0.53	gt1_site4_incl6_pt1
CH11	g inner core	128.45	207.06	464.65	257.59	78.60	-0.30	-0.21	0.14	0.44	grt2_site1_pt1
CH11	g inner core	128.74	207.54	464.95	257.41	78.80	-0.12	-0.01	0.63	0.74	g8_site2_incl5_pt1
CH11	g inner core	128.58	207.64	464.80	257.15	79.07	0.14	0.26	0.73	0.59	g8_site2_incl6_pt1
CH11	g inner core	128.49	206.77	464.55	257.78	78.28	-0.49	-0.53	-0.14	0.35	g8_site2_incl6_pt1b
CH11	g outer core	128.46	207.08	464.68	257.59	78.62	-0.30	-0.19	0.17	0.47	g1_site4_incl7_pt1
CH11	g outer core	128.40	206.91	464.56	257.65	78.51	-0.36	-0.30	0.00	0.36	g4_site1_incl1_pt1
CH11	g outer core	128.57	207.18	464.68	257.50	78.62	-0.20	-0.19	0.27	0.47	g4_site1_incl1_pt2
CH11	g outer core	128.45	207.24	464.65	257.41	78.79	-0.11	-0.02	0.33	0.44	g4_site1_incl1_pt3
CH11	g outer core	129.62	211.91	466.30	254.39	82.29	2.90	3.48	5.00	2.09	g4_site1_incl2_pt1
CH11	g outer core	128.60	207.45	464.72	257.27	78.84	0.03	0.03	0.54	0.51	g4_site1_incl3_pt1
CH11	g outer core	128.83	208.97	465.20	256.23	80.15	1.07	1.33	2.06	0.99	g4_site1_incl3_pt2
CH11	g outer core	128.05	206.37	464.48	258.11	78.32	-0.81	-0.49	-0.54	0.27	g4_site1_incl6_pt1
CH11	***g outer core (q around coe)***	***129.38***	***212.08***	***466.8***	***254.70***	***82.70***	***2.59***	***3.89***	***5.16***	***2.57***	***g5_site2_incl1_pt2rim***
CH11	***g outer core (q polycrystalline aggregates)***	***128.53***	***207.68***	***464.76***	***257.09***	***79.14***	***0.21***	***0.33***	***0.76***	***0.56***	***g5_site2_incl2_pt1***
CH11	***g outer core (q polycrystalline aggregates)***	***128.41***	***207.92***	***464.99***	***257.07***	***79.51***	***0.23***	***0.70***	***1.01***	***0.78***	***g5_site2_incl2_pt2***
CH11	***g outer core (q polycrystalline aggregates)***	***128.84***	***208.00***	***464.71***	***256.71***	***79.16***	***0.58***	***0.35***	***1.08***	***0.50***	***g5_site2_incl2_pt3***
CH11	g outer core	128.64	207.09	464.92	257.83	78.45	-0.53	-0.36	0.18	0.71	g8_site3_incl3_pt1
CH11	g outer core	128.78	208.47	465.10	256.62	79.69	0.67	0.88	1.56	0.89	g11b_site1_incl1_pt1
CH11	g outer core	128.82	207.93	465.10	257.17	79.11	0.13	0.30	1.02	0.89	g11b_site1_incl1_pt2
CH11	g outer core	128.57	208.23	465.03	256.81	79.66	0.49	0.85	1.32	0.83	g11b_site1_incl1_pt3
CH11	g outer core	129.07	209.00	465.68	256.68	79.93	0.62	1.12	2.09	1.47	g11b_site1_incl1_pt4
CH11	g outer core	129.07	208.41	465.09	256.68	79.34	0.62	0.53	1.49	0.88	g11b_site1_incl1_pt5
CH11	g outer core	129.08	209.77	465.63	255.86	80.69	1.43	1.88	2.86	1.42	g11b_site1_incl1_pt6
CH11	g outer core	128.85	207.07	465.03	257.97	78.22	-0.67	-0.59	0.16	0.83	g11b_site1_incl2_pt2
CH11	g outer core	128.28	205.73	464.30	258.57	77.45	-1.28	-1.36	-1.18	0.09	g11b_site1_incl2_pt3
CH11-2	g inner core	128.67	208.58	464.79	256.22	79.91	1.08	1.10	1.66	0.58	g3_site1_incl1_pt1
CH11-2	g inner core	128.85	209.07	464.91	255.85	80.22	1.45	1.41	2.16	0.70	g3_site1_incl1_pt2
CH11-2	g inner core	128.03	207.69	464.58	256.89	79.66	0.41	0.85	0.78	0.37	g3_site1_incl2_pt1
CH11-2	g inner core	129.98	212.52	466.25	253.73	82.55	3.57	3.74	5.61	2.04	g3_site1_incl4_pt1
CH11-2	g inner core	130.07	212.24	466.01	253.77	82.16	3.52	3.35	5.32	1.80	g3_site1_incl4_pt2
CH11-2	g inner core	128.39	207.24	464.38	257.14	78.85	0.16	0.04	0.33	0.17	g4_site5_incl1_pt1
CH11-2	g outer core	128.60	210.40	465.15	254.75	81.81	2.55	3.00	3.49	0.94	g4_site1_incl2_pt1
CH11-2	g rim	129.94	210.88	465.48	254.60	80.95	2.70	2.14	3.97	1.28	g2_site4_incl1_pt1
CH11-2	g rim	129.27	210.69	465.46	254.78	81.42	2.52	2.61	3.78	1.26	g4_site4_incl1_pt1
CH11-2	g rim	129.75	212.65	466.01	253.36	82.90	3.94	4.09	5.74	1.80	g4_site4_incl2_pt1
CH11-2	g rim	129.02	210.79	465.60	254.81	81.77	2.48	2.96	3.88	1.40	g4_site4_incl3_pt1
CH11-3	g rim	128.79	209.72	465.21	255.49	80.93	1.80	2.12	2.80	1.00	g3_site1_incl1_pt1
CH11-3	g rim	128.61	209.73	465.40	255.67	81.13	1.63	2.32	2.82	1.19	g3_site1_incl2_pt1
CH11-3	g rim	129.62	211.50	465.65	254.15	81.88	3.15	3.07	4.59	1.44	g3_site1_incl3_pt1
CH11-3	g rim	129.18	210.95	465.59	254.64	81.77	2.66	2.96	4.04	1.38	g3_site1_incl4_pt1
CH11-3	g rim	129.34	211.48	465.53	254.05	82.14	3.25	3.33	4.57	1.32	g3_site1_incl5_pt1
CH11-3	g rim	128.66	211.95	466.10	254.16	83.29	3.14	4.48	5.04	1.90	g3_site2_incl1_pt1
CH11-3	g rim	128.54	210.38	465.54	255.16	81.84	2.14	3.03	3.47	1.33	g1_site1_incl1_pt1
CH11-4	g outer core	128.65	208.30	464.67	256.37	79.65	0.93	0.84	1.39	0.46	g3_site2_incl1_pt1
CH11-4	g rim	128.06	206.66	464.07	257.41	78.61	-0.11	-0.20	-0.25	-0.14	g1_site1_incl2_pt1
CH11-4	g rim	128.03	207.68	464.32	256.64	79.65	0.66	0.84	0.77	0.11	g3_site1_incl1_pt1
CH11-4	g rim	128.54	208.87	464.67	255.80	80.34	1.50	1.53	1.96	0.46	g3_site1_incl2_pt1
CH11-4	g rim	128.25	207.42	464.46	257.04	79.17	0.26	0.35	0.51	0.25	g3_site1_incl3_pt1
CH11-4	g rim	128.30	207.25	464.24	256.99	78.95	0.31	0.14	0.34	0.03	g3_site1_incl4_pt1
CH11-4	g rim	129.08	209.86	465.24	255.38	80.78	1.92	1.97	2.94	1.03	g3_site1_incl5_pt1
CH11-4	g rim	129.08	211.23	465.78	254.55	82.15	2.75	3.34	4.32	1.57	g3_site1_incl6_pt1
CH11-5	g rim	128.69	209.21	465.13	255.93	80.51	1.37	1.70	2.30	0.93	g1_site3_incl1_pt1
CH11-5	g rim	128.71	211.73	466.40	254.67	83.02	2.63	4.21	4.82	2.20	g1_site3_incl2_pt1
CH11-5	g rim	129.28	212.43	466.46	254.04	83.14	3.26	4.33	5.51	2.26	g1_site3_incl2_pt2
CH11-5	g rim	128.62	209.80	465.18	255.37	81.19	1.92	2.37	2.89	0.97	g1_site1_incl1_pt1
CH11-5	g rim	130.09	214.69	467.35	252.66	84.61	4.64	5.80	7.78	3.14	g1_site1_incl2_pt1
CH11-5	g rim	130.30	215.58	467.77	252.19	85.28	5.11	6.47	8.67	3.56	g1_site1_incl2_pt2
CH11-5	g rim	129.56	214.01	466.81	252.80	84.46	4.50	5.64	7.10	2.61	g1_site1_incl3_pt1
CH11-5	g rim	128.54	211.20	465.78	254.59	82.66	2.71	3.85	4.28	1.58	g1_site1_incl4_pt1
CH11-6	g outer core	131.04	217.30	468.33	251.04	86.26	6.26	7.45	10.38	4.13	g3_site1_incl1_pt1
CH11-6	g rim	**130.74**	**218.32**	**468.88**	**250.56**	**87.58**	**6.74**	**8.77**	**11.41**	**4.67**	**g1_site1_incl2_pt1**
CH11-6	g rim	130.18	217.42	468.48	251.06	87.25	6.24	8.44	10.51	4.27	g1_site1_incl2_pt2

CH21-6 g rim							
Pinc from incl EoS = 5.44 ± 0.12 kbar							
Pinc from incl stiffness = 5.09 ± 0.09 kbar							
Ttrap_iso_eos (°C)	**Ptrap_iso_eos (kbar)**	**esd_Ptrap_iso_eos**	**Status_iso_eos**	**Ttrap_iso_CiJ (°C)**	**Ptrap_iso_Cij (lbar)**	**esd_Ptrap_iso_Cij**	**Status_iso_Cij**
500	14.1	0.2	ok	500	13.4	0.2	ok
505	14.1	0.2	ok	505	13.5	0.2	ok
510	14.2	0.2	ok	510	13.6	0.2	ok
515	14.3	0.2	ok	515	13.6	0.2	ok
520	14.3	0.2	ok	520	13.7	0.2	ok
525	14.4	0.2	ok	525	13.8	0.2	ok
530	14.5	0.2	ok	530	13.8	0.2	ok
535	14.5	0.2	ok	535	13.9	0.2	ok
540	14.6	0.2	ok	540	13.9	0.2	ok
545	14.6	0.2	ok	545	14.0	0.2	ok
550	14.7	0.2	ok	550	14.1	0.2	ok

Tab. S13 Results of the calculation of the entrapment isomeke with uncertainties. Both models ($P^{V}{}_{inc}$ obtained from the inclusion EoS and $P_{inc}{}^{strain}$ found with the stiffness tensor) have been used to get the residual pressure from the measured strain and calculate the entrapment isomeke. The uncertainties on the isomekes are estimated assuming an uncertainty equal to one standard deviation on the residual pressure

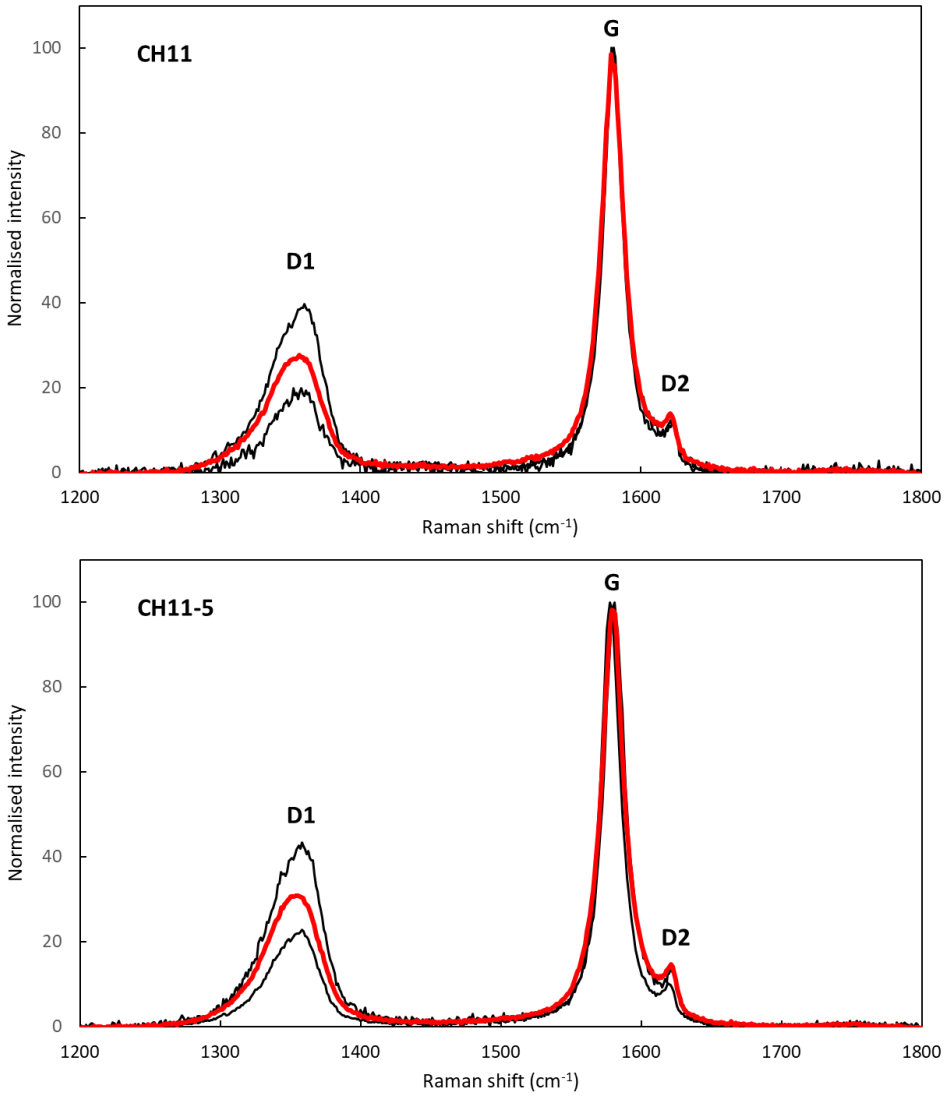

Fig. S9: Representative Raman spectra of carbonaceous material from sample CH11 (thin section CH11 and CH11-5). For each sample, the spectra corresponding to the maximum, minimum and intermediate temperatures are shown.

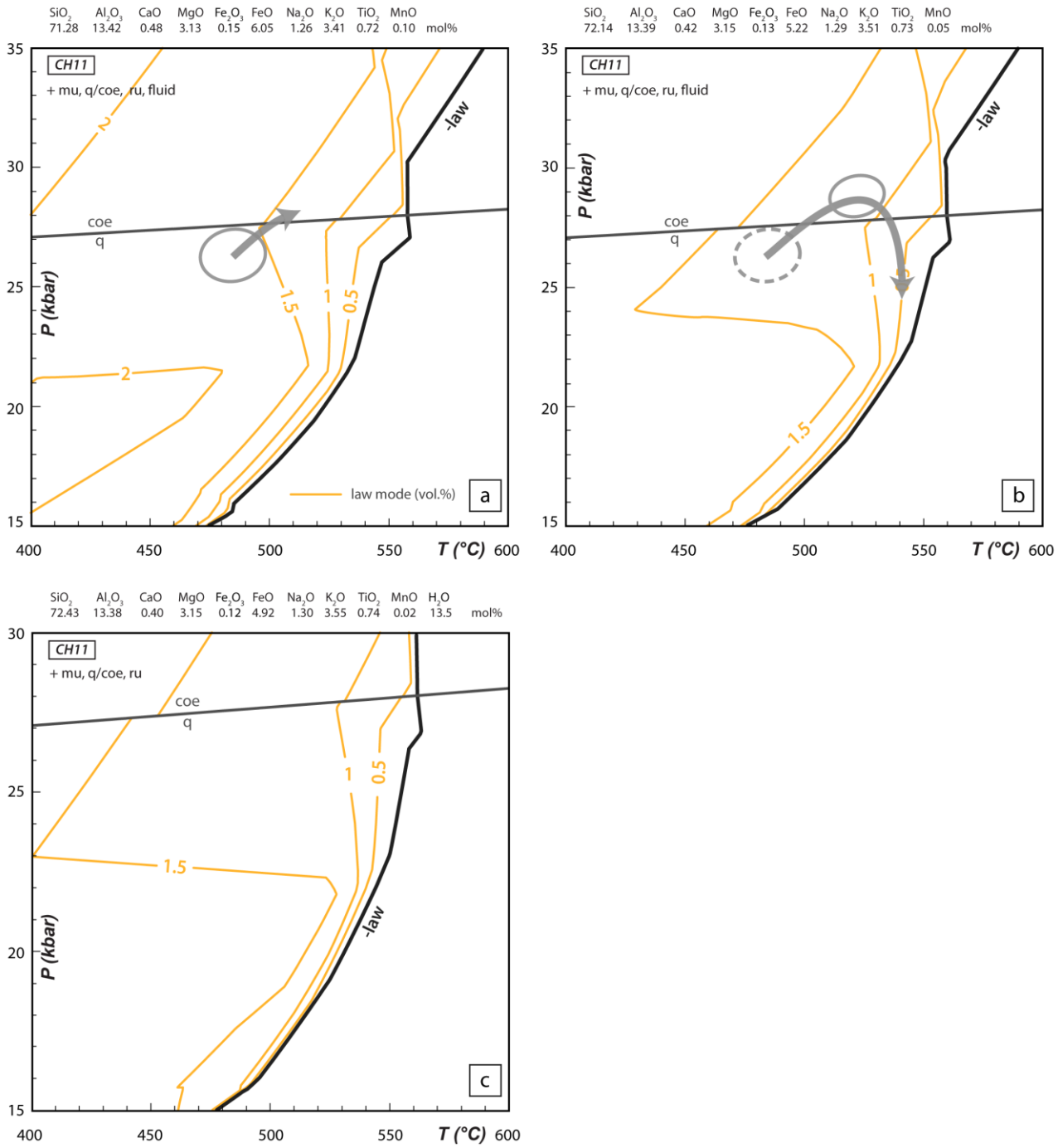

Fig. S10: Modal amount of lawsonite calculated with the unfractionated bulk composition (**a**), subtracting the composition of garnet inner core from the measured bulk composition (**b**), and subtracting the composition of garnet inner and outer core from the measured bulk composition (**c**). The grey circles and the arrow indicate the *P*–*T* conditions for the growth of garnet inner and outer core, as inferred from Figure 10

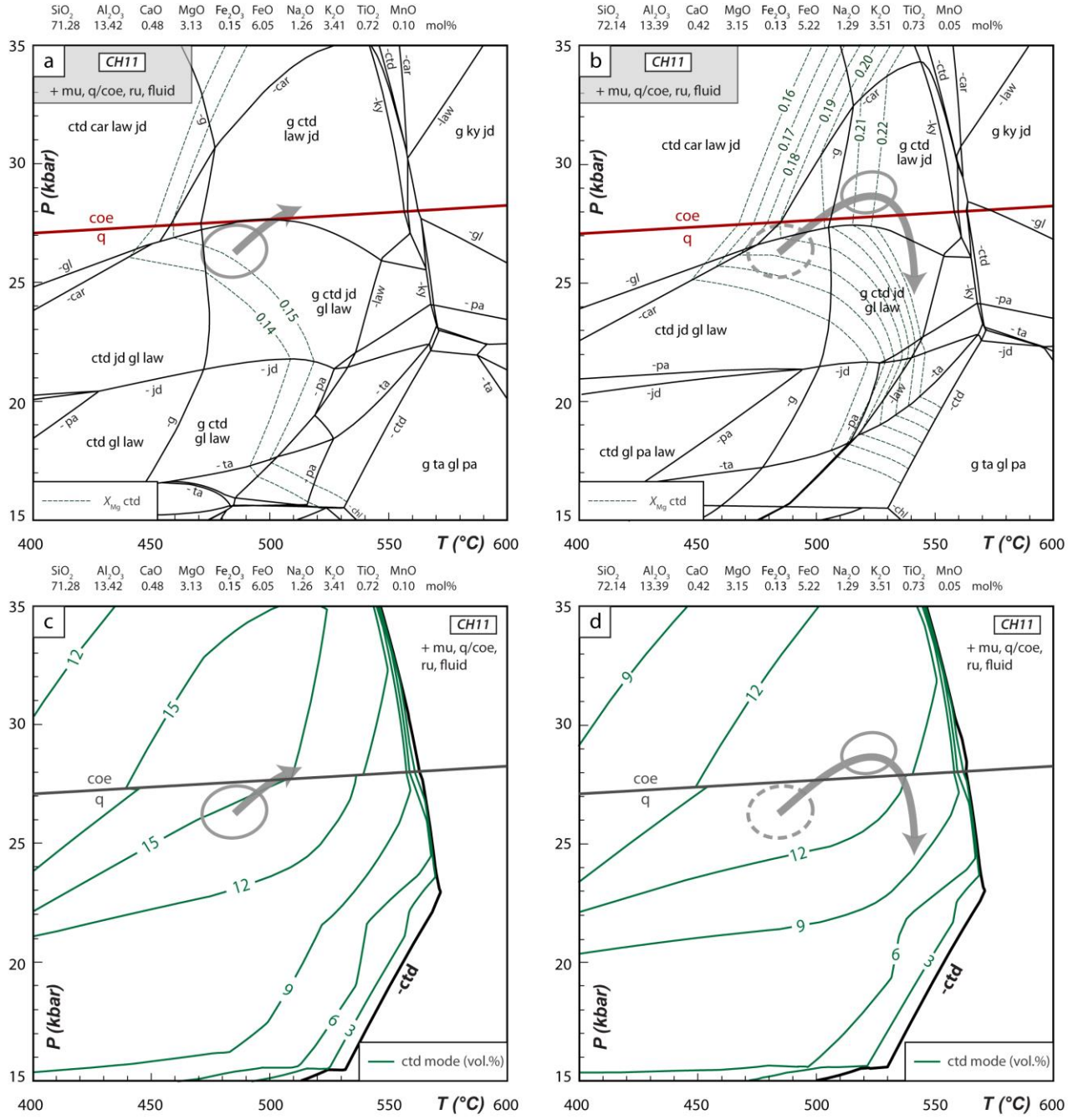

Fig. S11: X_{Mg} isopleths for chloritoid for the H_2O-saturated *P*–*T* pseudosections calculated for sample CH11 using the unfractionated bulk-rock composition (**a**) and a composition from which the garnet inner core has been subtracted (**b**). Some fields are not labelled for the sake of clarity; their assemblages can be deduced from the assemblages in adjacent fields. The grey circles indicate the *P*–*T* conditions for the growth of garnet inner and outer core. The grey arrow is the inferred prograde *P*–*T* path. **c**, **d** Chloritoid modal amount calculated for (**a**) and (**b**), respectively.

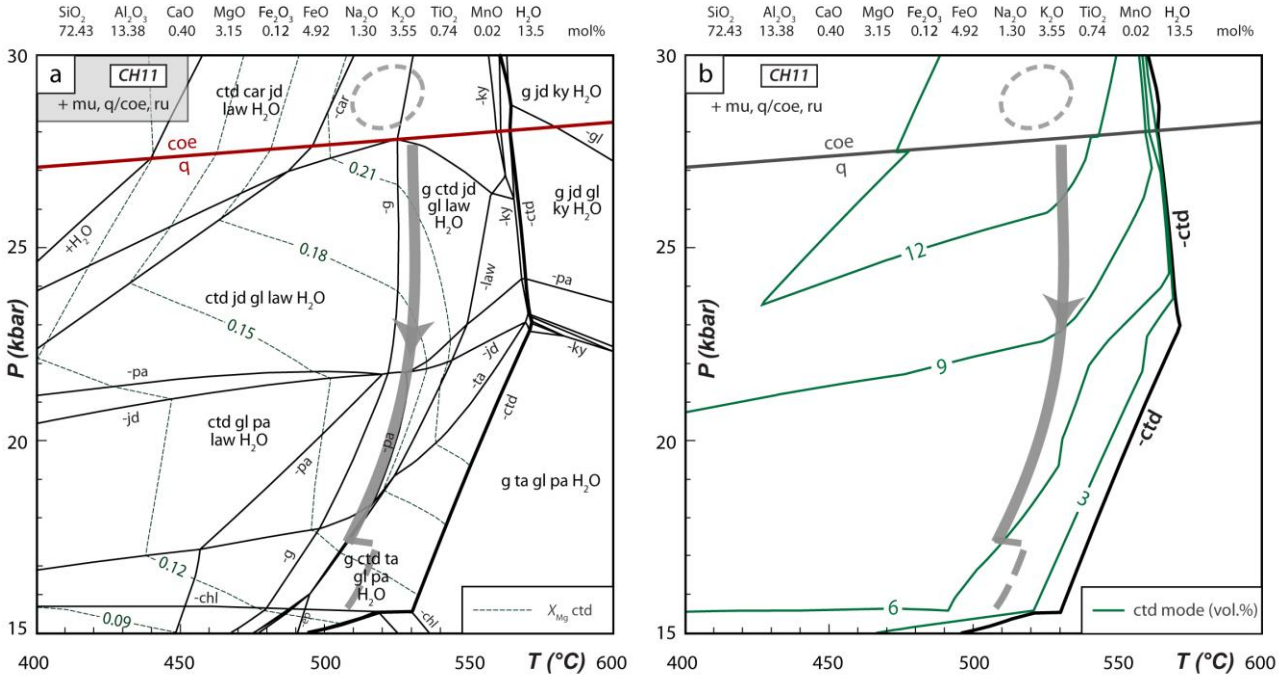

Fig. S12: a X_{Mg} isopleths for chloritoid for the *P*–*T* pseudosection calculated for the sample CH11, considering progressive garnet fractionation. *P*–*T* pseudosection is calculated in the range 15–30 kbar and 400–600 °C, using a fixed amount of H_2O and the bulk-rock composition obtained by garnet core (inner and outer) fractionation. **b** Chloritoid modal amount for the same *P*–*T* pseudosection. The grey arrow in (**a**) and (**b**) is the inferred *P*–*T* path followed during the growth of garnet rim.

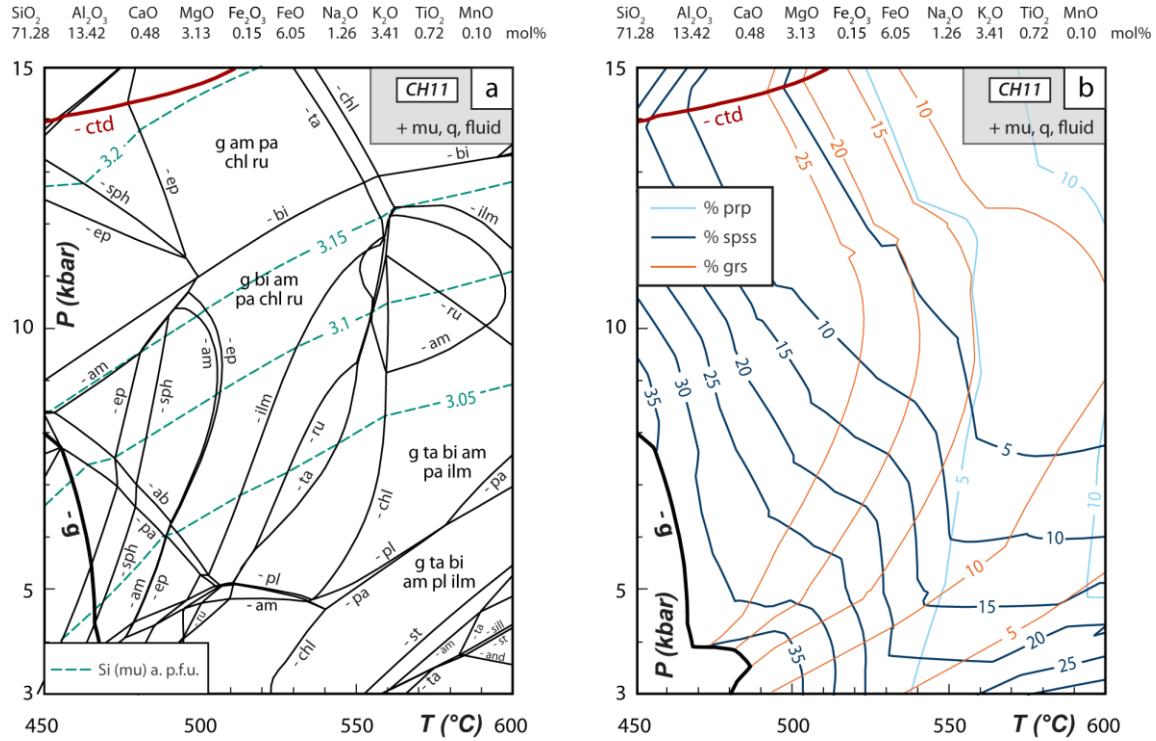

Fig. S13: H_2O-saturated *P–T* pseudosection calculated for sample CH11 using the unfractionated bulk-rock composition (Tab. S6) in the range 3–15 kbar and 450–600 °C. (**b**) Garnet isopleths calculated for (a). Colours for the garnet isopleths correspond to the ones used for the chemical profile in Figure 9

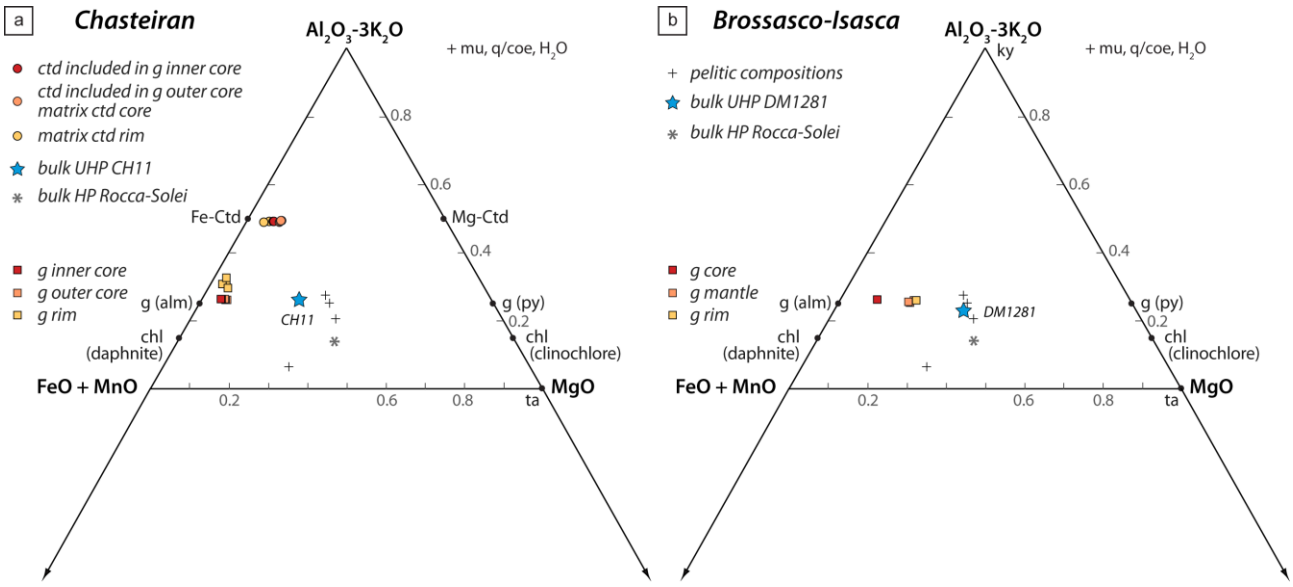

Fig. S14: a AFM diagram showing the bulk-rock composition of the studied sample CH11 from the UHP Chasteiran Unit projected from muscovite, quartz, and H_2O. Chemical compositions of garnet (inner and outer core, and rim) and chloritoid (core and rim) analysed in this sample are also plotted. Compositions of a metapelite from the HP Rocca-Solei Unit in the Dora-Maira Massif (Groppo et al. 2019) and from mean pelites of Shaw (1956), Mahar et al. (1997), Tinkham et al. (2001), and Spear and Pyle (2010) are also plotted. **b** AFM diagram showing the bulk-rock composition of a metapelite from the UHP Brossasco-Isasca Unit (Groppo et al. 2019) projected from muscovite, quartz, and H_2O. Representative chemical compositions of garnet core, mantle, and rim (Groppo et al. 2019) analysed in this sample are also plotted. Compositions of a metapelite from the HP Rocca-Solei Unit in the Dora-Maira Massif (Groppo et al. 2019) and from mean pelites of Shaw (1956), Mahar et al. (1997), Tinkham et al. (2001), and Spear and Pyle (2010) are also plotted

References

Armstrong JT (1988) Quantitative analysis and oxide materials: comparison of Monte Carlo, ZAF and J(rZ) procedures. In: Newbury DE (Ed) Microbeam analysis. San Francisco Press 239–246

Armstrong JT (1991) Quantitative elemental analysis of individual microparticles with electron beam instruments. In: Heirich KFS, Newbury DE (eds) Electron Probe Quantitation. Plenum Press 261–315

Beyssac O, Goffé B, Chopin C, Rouzaud JN (2002) Raman spectra of carbonaceous material in metasediments: a new geothermometer. J Metamorph Geol 20:859–871

Beyssac O, Goffé B, Petitet JP, Froigneux E, Moreau M, Rouzaud JN (2003) On the characterization of disordered and heterogeneous carbonaceous materials using Raman spectroscopy. Spectrochim Acta A 59:2267–2276

Carignan J, Hild P, Mevelle G, Morel J, Yeghicheyan D (2001) Routine analyses of trace elements in geological samples using flow injection and low pressure on-line liquid chromatography coupled to ICP-MS: a study of geochemical reference materials, BR, DRN, UB-N, AN-G and GH. Geostandards Newslett 25:187–198

de Capitani C, Brown TH (1987) The computation of chemical equilibrium in complex systems containing non-ideal solutions. Geochim Cosmochim Acta, 51:2639–2652

de Capitani C, Petrakakis K (2010) The computation of equilibrium assemblage diagrams with Theriak/Domino software. Amer Miner 95:1006–1016

Holland, TJB, Powell, R (2011) An improved and extended internally consistent thermodynamic dataset for phases of petrological interest, involving a new equation of state for solids. J Metamorph Geol 29:333–383

Groppo C, Ferrando S, Gilio M, Botta S, Nosenzo F, Balestro G, Festa A, Rolfo F (2019) What's in the sandwich? New P–T constraints for the (U)HP nappe stack of southern Dora-Maira Massif (Western Alps). Eur J Mineral 31:665–683

Holland TJB Powell R (2003) Activity–composition relations for phases in petrological calculations: an asymmetric multicomponent formulation. Contrib Mineral Petrol 145:492–501

Mahar EM, Baker J, Powell R, Holland TJB, Howell N (1997) The effect of Mn on mineral stability in metapelites. J Metamorph Geol 15:223-238

Pouchou JL, Pichoir F (1985) "PAP" $\phi(\rho Z)$ procedure for improved quantitative microanalysis. In: Armstrong JT (ed) Microbeam Analysis. San Francisco Press, San Francisco, CA, pp 104–106

Shaw DM (1956) Geochemistry of pelitic rocks: Part III. Major elements and general geochemistry. Bull Geol Soc Am 67:919-934

Spear FS, Pyle JM (2010) Theoretical modelling of monazite growth in a low-Ca metapelite. Chemical Geology 273:111-119

Tinkham DK, Zuluaga CA, Stowell HH (2001) Metapelite phase equilibria modeling in MnNCKFMASH: the effect of variable Al_2O_3 and Mg/(MgO+FeO) on mineral stability. Geol Mat Res 3:1-41

Wei CJ Powell R (2004) Calculated phase relations in high-pressure metapelites in the system NKFMASH (Na_2OK_2O–FeO–MgO–Al_2O_3–SiO_2–H_2O). J Petrol 45:183–202

White RW, Powell R, Holland TJB, Worley BA (2000) The effect of TiO_2 and Fe_2O_3 on metapelitic assemblages at greenschist and amphibolite facies conditions: mineral equilibria calculations in the system K_2O-FeO-MgO-Al_2O_3-SiO_2-H_2O-TiO_2-Fe_2O_3. J Metamorph Geol 18:497–511

White RW, Powell R, Clarke GL (2002) The interpretation of reaction textures in Fe-rich metapelitic granulites of the Musgrave Block, central Australia: constraints from mineral equilibria calculations in the system K_2O–FeO–MgO–Al_2O_3–SiO_2–H_2O–TiO_2–Fe_2O_3. J Metamorph Geol 20:41–55

White RW, Powell R, Holland TJB, Worley B (2000) The effect of TiO_2 and Fe_2O_3 on metapelitic assemblages at greenschist and amphibolite facies conditions: mineral equilibria calculations in the system K_2O–FeO–MgO–Al_2O_3–SiO_2–H_2O–TiO_2–Fe_2O_3. J Metamorph Geol 18:497–511

White RW, Powell R, Johnson TE (2014a) The effect of Mn on mineral stability in metapelites revisited: new a–x relations for manganese-bearing minerals. J Metamorph Geol 32:809–828

White RW, Powell R, Holland TJB, Johnson TE, Green ECR (2014b) New mineral activity–composition relations for thermodynamic calculations in metapelitic systems. J Metamorph Geol 32:261–286